arXiv:1602.05325v2 [astro-ph.GA] 3 Mar 2016

Galactic Center Mini-spiral by ALMA - Possible Origin of the Central Cluster

Masato Tsuboi[1,3], Yoshimi Kitamura[1], Makoto Miyoshi[2], Kenta Uehara[3], Takahiro Tsutsumi[4] and Atsushi Miyazaki[2,5]

[1]Institute of Space and Astronautical Science, Japan Aerospace Exploration Agency, 3-1-1 Yoshinodai, Chuo-ku, Sagamihara, Kanagawa 252-5210, Japan

[2]National Astronomical Observatory of Japan, Mitaka, Tokyo 181-8588, Japan

[3]Department of Astronomy, The University of Tokyo, Bunkyo, Tokyo 113-0033, Japan

[4]National Radio Astronomy Observatory, Socorro, NM 87801-0387, USA

[5]Japan Space Forum, Kandasurugadai, Chiyoda-ku,Tokyo,101-0062, Japan

*E-mail: tsuboi@vsop.isas.jaxa.jp

Received ⟨20-Jan-2016⟩; Accepted ⟨03-Mar-2016⟩

Abstract

We present continuum images of the "Galactic Center Mini-spiral" of 100, 250, and 340 GHz bands with the analysis of the Cy.0 data acquired from the Atacama Large Millimeter/submillimeter Array (ALMA) archive. Pretty good UV coverage of the data and the "self-calibration" method give us an opportunity to obtain dynamic ranges of over 2×10^4 in the resultant maps of the 250 and 340 GHz bands. In particular the image of the 340 GHz band has high dynamic ranges unprecedented in sub-millimeter wave. The angular resolutions attain to $1.57'' \times 1.33''$ in the 100 GHz band, $0.63'' \times 0.53''$ in the 250 GHz band, and $0.44'' \times 0.38''$ in the 340 GHz band, respectively. The continuum images clearly depict the "Mini-spiral", which is an ionized gas stream in the vicinity of Sgr A*. We found the tight correlation between the dust emission peaks and the OB/WR stars in the Northern-arm of the "Mini-spiral". The core mass function of the dust core identified by the *clumpfind* algorithm would obey the flat power-law $dN/dM \propto M^{-1.5\pm0.4}$ on the high-mass side. These support the scenario that the star forming cloud has fallen into the immediate vicinity of Sgr A* for the origin of the Central cluster.

Key words: Galaxy: center$_1$ — stars: formation$_2$ — ISM: dust$_3$

1 Introduction

The Galactic center region is the nucleus of the nearest spiral galaxy; the Milky Way. Sagittarius A* (Sgr A*) is a compact source from radio to X-ray located near the dynamical center of the galaxy and is associated with the Galactic central supermassive black hole (GCBH). The mass of the GCBH is estimated to be $M_{\rm GC} \simeq 4 \times 10^6 M_\odot$ from infrared (IR) astrometry observations (e.g. Ghez et al. 2008, Gillessen et al. 2009). The region surrounding Sgr A* is recognized to be a laboratory for peculiar phenomena, which will be found in the nuclei of normal galaxies by future telescopes. In the last two decades, young and highly luminous clusters have been found in the Central Molecular Zone (CMZ) (Morris & Serabyn 1996) by IR observations (e.g. Genzel et al. 1996, Figer et al. 1999, Figer et al. 2002). These bright star clusters except for the Central cluster presumably formed in the cradle dense molecular clouds in the CMZ. However, the Central cluster is a unique object in the Milky Way because the cluster is centered at Sgr A* and concentrates within $r \sim 0.5$pc. The cluster contains ~ 100 OB and WR stars (e.g. Genzel et al. 1996). It may be difficult to make the Central cluster in a way by which stars are usually formed in the disk region because of the following reasons. First, the tidal force of Sgr A* must have a serious effect on the star formation since the minimum number H_2 density for stabilization toward the tidal shearing is $n(\mathrm{H_2}) \gtrsim 3 \times 10^8$ cm^{-3} at $r \sim 0.5$pc (Christopher et al. 2005, Tsuboi et al. 2011). Second, the strong Lyman continuum radiation from the early type stars in the cluster ionizes rapidly the ISM in the region. The ionized ISM stream is identified as the "Galactic Center Mini-spiral" surrounding Sgr A*(Ekers et al. 1983, Lo& Claussen 1983), of which elongated appearance and kinematics indicate that it is a tentative structure. Therefore, it is still an open question how the Central cluster has formed.

Two distinct scenarios for the formation of the Central cluster have been proposed so far. One is current in-situ star formation in such extreme environment of the vicinity of Sgr A*. The other is that a molecular cloud is fallen from the region somewhat far from Sgr A* to the vicinity of Sgr A* after star formation in the cloud started (e.g. Tsuboi et al. 2015b). Recently a high-resolution observation ($0.088'' \times 0.046''$) within $30''$ of Sgr A* at 34 GHz with JVLA detected many sources with bow-shock appearance (Yusef-Zadeh et al. 2015a). The authors explained them as ionized outer envelopes of newly forming low mass stars. If so, this may be circumstantial evidence of the in-situ

star formation near Sgr A*. However, the elapsed time for falling from $r \sim 10$ pc to the vicinity of Sgr A* in the second scenario is 10^5 yr, comparable to the ages of protostars in the Galactic disk region. The low mass stars may remain as protostars if the low mass star formation in the falling cloud is as slow as that in the Galactic disk region. Consequently, the JVLA-detected sources do not necessarily support the first scenario of the current in-situ star formation near Sgr A* (also see Paumard et al. 2006).

The detailed observations of the survived molecular gas or partially ionized gas are necessary to understand the star formation in the the vicinity of Sgr A*. Recently SiO(5-4) emission line observations detected several spots of molecular gas around Sgr A*. However the association between the spots and the IR-detected stars are not clear (Yusef-Zadeh et al. 2013, Yusef-Zadeh et al. 2015b). We analyze the ALMA Cy.0 data of the region to depict the dust emission from the molecular cloud in the high resolution less than $1''$. Using them, we can trace the molecular cloud before destructed completely by the UV continuum radiation. Throughout this paper, we adopt 8.5 kpc as the distance to the Galactic center. Then, $1''$ corresponds to about 0.04 pc at the distance.

2 Data Analysis and Results

We analyze the Cy.0 data of the Sgr A* region in 100-, 250-, and 340-GHz bands, which was acquired from the ALMA archive (ADS/JAO.ALMA#2011.0.00887.S). Nineteen 12-m antennas were available. In addition, the epoch, May 18, 2012, was suitable for imaging observation because Sgr A* was in a relatively quiet phase (Brinkerink et al. 2015). Since the original observation aimed for the measurement of the time variation of Sgr A*, the time span of the observation is longer than 7 hrs (from 03:30:47 UT to 10:52:16 UT). Each frequency band has four spectral windows. The band width of the spectral window is 1.875 GHz. The fields of view (FOVs) are centered at Sgr A*, $\alpha_{\rm J2000} = 17^h45^m40^s.04$, $\delta_{\rm J2000} = -29^\circ00'28''.10$. NRAO530 and J1924-292 were used as phase calibrators. The flux density scale was determined using Titan and Neptune.

Further data calibration and imaging of the archival data were done by classic VLBA AIPS(NRAO) using the self-calibration method. First we removed residual fringe rates and delays of the raw visibility by the task FRING, which was found to be quite effective. Second the residual complex gain errors of the data were minimized using the "self-calibration" method in the software. The good UV coverage and "self-calibration" method give us an opportunity to obtain high dynamic range in the resultant maps.

Fig. 1 shows the intensity map of the 100 GHz band. Here, we combined the four spectral window maps of $f_c = 93, 95, 105,$ and 107 GHz in the 100 GHz band to improve the sensitivity. The

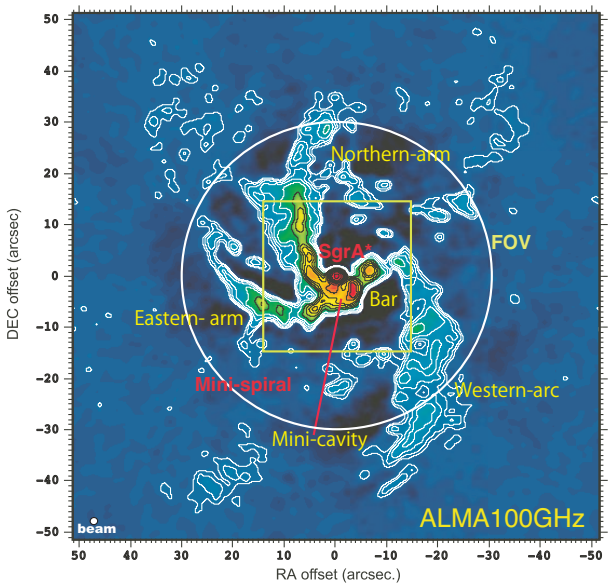

Fig. 1. ALMA map in the 100 GHz band of the "Mini-spiral" including Sgr A*. The four spectral windows of $f_c = 93, 95, 105,$ and 107 GHz are combined to improve the sensitivity. The diameter of the FOV is $60''$. The angular resolution is $1.57'' \times 1.33''$ at $PA = 74^\circ$, which is shown as an oval on the left bottom corner. The rms noise level is 0.33 mJy beam^{-1}, and the contour levels are 0.63, 1.3, 2.5, 5.0, 7.5, 10, 20, 30, 40, 50, 100, 200, 300, 400, 500, 1000, and 2000 mJy beam^{-1}. The flux density of Sgr A* is $S_\nu = 2.35 \pm 0.19$ Jy at 100 GHz. The square shows the area covered by Fig.2.

figure size is $100'' \times 100''$. The resultant Full Width at Half Maximum (FWHM) beam is $1.57'' \times 1.33''(PA = 74^\circ)$, which corresponds to $0.065\mathrm{pc} \times 0.055\mathrm{pc}$ at the Galactic center. The diameter of the FOV is $D_{\mathrm{FOV}} = 60''$ or 2.5 pc. This means that the sensitivity of the map decreases to 50% at the edge of the FOV, which is caused by the beam pattern of the element antenna. The correction for the primary beam attenuation is not applied to the map. Features with spatial scales larger than $38''$ or 1.6 pc were resolved out. The rms noise level is $S_\nu = 0.33$ mJy beam^{-1} (4ch-combined) at the map center. The flux density of Sgr A* is $S_\nu = 2.35 \pm 0.19$ Jy at 100 GHz. The error includes the calibration error. The "Mini-spiral" is clearly seen in this map, which has the "Eastern- arm", the "Northern-arm", the "Bar", and the "Western-arc" as substructures. Moreover, the "Mini-cavity" is identified on the Bar. Because the continuum emission at 100 GHz is originated mainly from the ionized ISM, the appearance closely resembles that at centimeter wave (e.g. Yusef-Zadeh & Morris 1987).

The left and right panels of Fig.2 show the intensity maps of the 250 and 340 GHz bands, respectively. Both figures cover a $29'' \times 29''$ area centered at Sgr A*. For the left panel, there are four spectral windows of $f_c = 245, 247, 257,$ and 259 GHz in the 250 GHz band and the four data

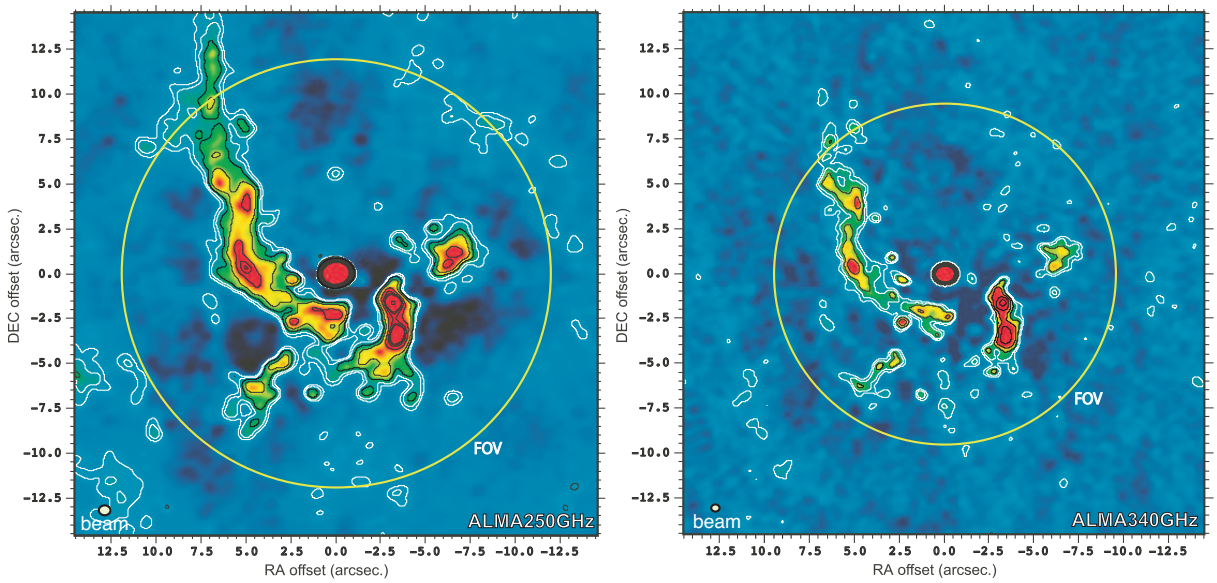

Fig. 2. left panel: ALMA map in the 250 GHz band of the "Mini-spiral" including Sgr A*. The four spectral windows of $f_c = 245, 247, 257$, and 259 GHz are combined to improve the sensitivity. The diameter of the FOV is $24''$ (circle). The angular resolution is $0.63'' \times 0.53''$ at $PA = -84^\circ$, which is shown as an oval on the left bottom corner. The rms noise level is 0.13 mJy beam^{-1}, and the contour levels are 0.31, 0.63, 1.3, 2.5, 5.0, 10, 20, 30, 40, 50, and 75 mJy beam^{-1}. The flux density of Sgr A* is $S_\nu = 3.55 \pm 0.35$ Jy at 250 GHz. **right panel**: ALMA map in the 340 GHz band of the same region as the left panel. The four spectral windows of $f_c = 336, 338, 348$, and 350 GHz are combined to improve the sensitivity. The diameter of the FOV is $18''$ (circle). The angular resolution is $0.44'' \times 0.38''$ at $PA = -89^\circ$, which is shown as an oval on the left bottom corner. The rms noise level is 0.33 mJy beam^{-1}, and the contour levels are the same as in the left panel. The flux density of Sgr A* is $S_\nu = 3.44 \pm 0.51$ Jy at 340 GHz.

sets are combined to improve the sensitivity. The diameters of the FOV is $D_{\rm FOV} = 24''$ or 1 pc. The correction for the attenuation of the primary beam is not applied to the map. The resultant FWHM beam is $0.63'' \times 0.53''(PA = -84^\circ)$, or $0.026{\rm pc} \times 0.022{\rm pc}$ at the Galactic center. Features with spatial scales larger than $15''$, or 0.63 pc, were resolved out. The rms noise level at the map center is $S_\nu = 0.13$ mJy beam^{-1} at 250 GHz. The good UV coverage and "self-calibration" give us to obtain high dynamic range of 2.7×10^4 in the resultant map. The flux density of Sgr A* is $S_\nu = 3.55 \pm 0.35$ Jy at 250 GHz. Because the light curves at 250 and 340 GHz show that Sgr A* has considerable variability, the quoted values are considered as the time-averaged flux densities at this epoch. The error includes the calibration error.

For the right panel, there are four spectral windows of $f_c = 336, 338, 348$, and 350 GHz in the 340 GHz band and the four data sets are also combined to improve the sensitivity. The diameters of the FOV is $D_{\rm FOV} = 18''$, or 0.75 pc. The correction for the attenuation of the primary beam is not applied to the map. The resultant FWHM beam at 340 GHz is $0.44'' \times 0.38''(PA = -89^\circ)$, which corresponds to $0.018{\rm pc} \times 0.016{\rm pc}$. Features with spatial scales larger than $11''$, or 0.46 pc, were resolved out. The

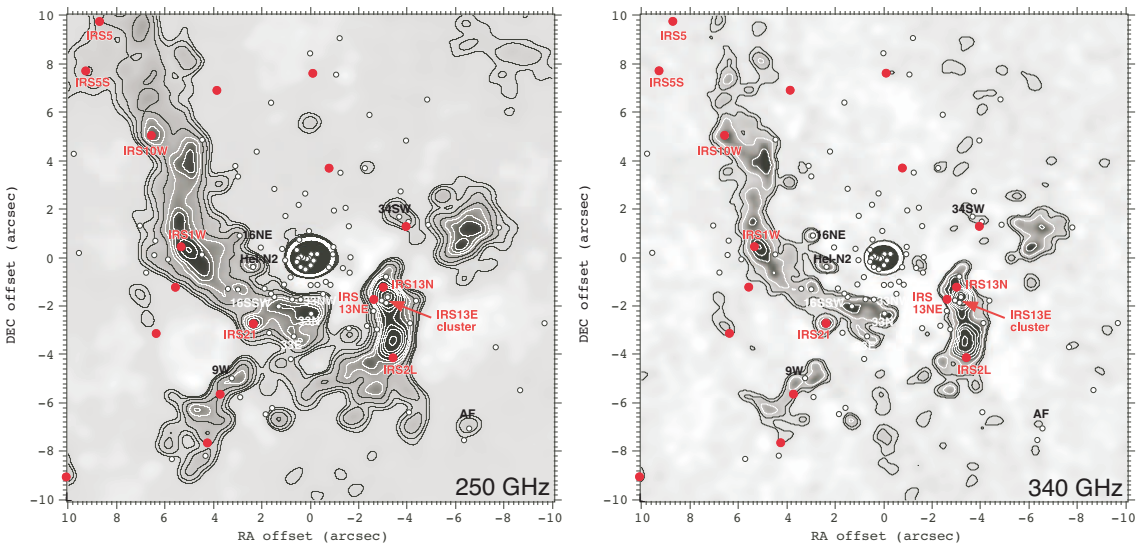

Fig. 3. Positions of the early type stars detected by IR observations are plotted by the circles on the ALMA maps at 250 GHz (left) and 340 GHz (right). IRS1W, IRS2L, IRS5, IRS10W, IRS13EN, IRS13N, and IRS21, which are known as "bow-shock" stars designated by the filled circles. They are located on the dust emission peaks or within $0.5''$ of them in the Northern-arm and the Bar. The other early type stars are designated by the open circles. IRS9W, IRS16NE, IRS16SSW, IRS33E, IRS33N, IRS33NW, IRS34SW, HeI-N2, and AF are also located on the dust emission peaks or within $0.5''$ of them.

rms noise level at the map center is $S_\nu = 0.15$ mJy beam^{-1} at 340 GHz. The dynamic range in the resultant map reaches to 2.3×10^4, which is unprecedented at that frequency. The flux density of Sgr A* is $S_\nu = 3.44 \pm 0.51$ Jy at 340 GHz.

The Northern-arm, the western half of the Eastern-arm, and the Bar are clearly seen both in the figures at 250 and 340 GHz. The Mini-cavity is clearly identified around $\Delta\alpha = -1.5''$, $\Delta\delta = -2.0''$ (Cf. Fig. 6 in Zhao et al. 2009). While the Eastern-half of the Eastern-arm is fairly in the FOV at 250 GHz, it is out of the FOV at 340 GHz. The Western-arc is out of both the FOVs. The Northern-arm seems to have a helical appearance in the both figures (Cf. Fig. 22 in Zhao et al. 2009). Moreover, we find many smaller components both in the figures, which have statistical significance of $> 5\sigma$. Because the data in the two bands have different UV coverage, these small objects are real substructures rather than artifacts caused by the side lobes. However, these are not associated with the SiO sources detected by ALMA (Yusef-Zadeh et al. 2013, Yusef-Zadeh et al. 2015b).

3 Discussion

The continuum emission at 340 GHz can be considered as the dust thermal emission for the following reason. The widths of the Northern-arm at 250 and 340 GHz seem to be narrower than that at 100 GHz. In the later, the Northern-arm has a "spine" structure and a relatively smooth envelope structure around it. While the Northern-arm at 250 and 340 GHz has only a "spine"

structure structure (see Fig.1 and Fig. 2). The beam-deconvolved widths at $\Delta\delta = 2.7 - 3.9''$ are $\theta = \sqrt{(Gaussian\ fit\ width)^2 - b_{maj.} \times b_{min.}} = 1.30 \pm 0.03''$ at 250 GHz and $\theta = 1.15 \pm 0.05''$ at 340 GHz although the width is $\theta = 1.86 \pm 0.02''$ at 100 GHz. The beam sizes at the three bands are much smaller than the arm widths. In addition, the resolve-out limits at the three bands are much larger than the arm widths. Then the difference among the widths is not caused by the beam size difference and/or the resolve-out limit difference. While the continuum emission at 100 GHz of the Mini-spiral is thought to mainly come from ionized gas, the continuum emission at 340 GHz presumably comes from dust although that at 250 GHz may be a mixture of free-free emission from ionized gas and dust emission. The observed "spine" structure presumably shows the dust ridge in the Mini-spiral. On the other hand, the envelope structure probably shows the distribution of the ionized gas oozing from the ridge by strong UV radiation.

To explore the relation between the dust ridge of the Mini-spiral and the OB/WR stars of the Central cluster (e.g. Genzel et al. 1996, Paumard et al. 2006, Zhao et al. 2009), we show the positions of the stars on the emission maps at 250 and 340 GHz in the left and right panels of Fig.3, respectively. More than 10 early type stars are located on the dust emission peaks in the Northern-arm and the Bar. The "bow-shock" stars, which have shell-like envelopes, were found in recent IR observations (e.g. Sanchez-Bermudez et al. 2014). IRS1W, IRS2L, IRS5, IRS10W, IRS13EN, IRS13N, and IRS21 seem to lie along the Northern-arm and the Bar. Moreover, they are located on the dust emission peaks or within $0.5''$ of them except for IRS 5, which is out of the FOV at 340 GHz. Other early type stars, IRS16NE, IRS16SSW, IRS33E, IRS33N, IRS33NW, IRS34SW, HeI-N2, and AF, are also located on the dust emission peaks or within $0.5''$ of them. In addition, the "famous" massive dense star cluster, IRS13E, is located on the center of the brightest dust condensation in the Bar (e.g. Schödel et al. 2005). There seems to be tight correlation between the dust emission peaks and the OB/WR stars in the Northern-arm and the Bar. On the other hand, the correlation between the Eastern-arm and the OB stars except for IRS9W is not clear because of the limitation of the FOV.

As the next step of the quantitative analysis of the dust emission, we search dust clumps in the 340 GHz continuum map using the *clumpfind* algorithm (Williams et al. 1994). We detected 18 clumps within the FOV at 340 GHz. To estimate the clump mass, M_c, from the integrated intensity at 340 GHz, F_{340}, we use the formula for optically thin thermal emission from dust, $M_c = F_\nu d^2 / \kappa_\nu B_\nu(T_d)$, where κ_ν is the dust mass absorption coefficient, $\kappa_\nu = 0.1 \times (\nu/1200GHz)^\beta$ (Hildebrand 1983). We assume here the dust temperature of $T_d = 20$ K as a conservative value, $\beta = 2$, and the metallicity of $Z/Z_0 = 1$. The most massive core has ~ 170 M$_\odot$. When we get a new dust temperature of the clump, T'_d, the clump mass changes to $(B_\nu(20)/B_\nu(T'_d))M_c \sim (20/T'_d)M_c$ because of $h\nu/kT < 1$. Assuming a spherical dust particle, we estimate the mean number density

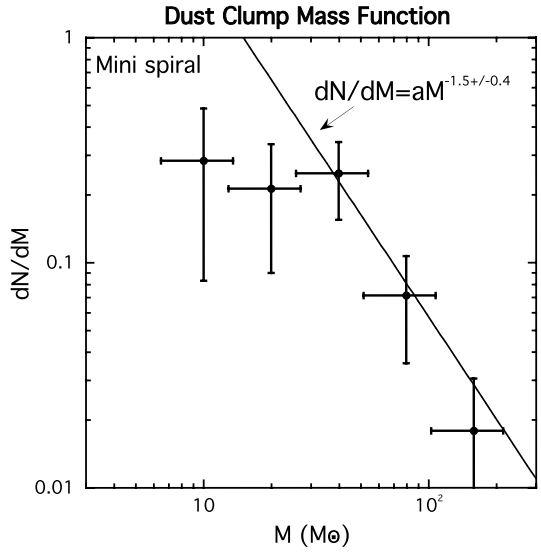

Fig. 4. Dust clump mass function (CMF) of the Mini-spiral at 340 GHz. The solid line shows the best-fit power-law function for massive three data points, $dN/dM \propto M^{-1.5\pm0.4}$.

using $\bar{n} = M_c/\mu m_H/\frac{4\pi}{3}r_c^3$, where μ is the mean molecular weight, $\mu = 2.3$. The physical parameters of the clumps are shown in table 1. Fig.4 shows the dust clump mass function (CMF). The function on the high-mass side seems to obey a power-law, which is usually used to depict the CMFs in the disk region of the Galaxy. The solid line in the figure shows the best-fit function for massive three data points, $dN/dM \propto M^{-1.5\pm0.4}$. Recent IR observations suggested that the stars in the vicinity of Sgr A* have continuously formed with a top-heavy IMF (e.g. Maness et al. 2007). Although the slope of the Mini-spiral CMF on the high-mass side is steeper than that of the expected top-heavy IMF of the Central cluster, the steeper CMF can change into the flat IMF by the tidal shear of Sgr A*. The mean gas number densities of the dust clumps are fairly less than the minimum gas density required for stability against the tidal shear of the Sgr A* (Tsuboi et al. 2015). The protostars already formed in the cloud could grow to stars finally because the typical number density of the protostars is larger than the minimum gas density, on the other hand the remaining cloud gas will be ruined by the tidal shear. Consequently the IMF should become flatter than the CMF because the tidal destruction is more effective for lower mass cores.

Based on the observed tight correlation between the dust emission peaks and the OB/WR stars in the Northern-arm and the properties of the detected dust clumps, we would propose the following scenario as the origin of the Central cluster; The stars including massive stars have formed in a

Table 1. Dust Clumps in the "Mini-spiral".

RA offset[a] ($''$)	DEC offset[a] ($''$)	d^b (pc)	M_c ($M_\odot$)	$\bar{n}$ (cm^{-3})	n^c_{min} (cm^{-3})
3.43	0.984	0.147	10.2	6.4e+06	1.6e+10
7.38	-3.02	0.329	12.5	3.0e+06	1.4e+09
-2.83	-5.52	0.256	15.9	6.3e+06	3.0e+09
0.02	-7.52	0.310	19.3	1.9e+06	1.7e+09
2.88	-2.52	0.158	24.1	5.6e+06	1.3e+10
6.28	2.48	0.278	28.5	6.5e+06	2.3e+09
3.43	-1.02	0.147	34.1	2.6e+06	1.6e+10
1.67	-2.02	0.108	35.2	8.6e+06	4.0e+10
0.02	-2.52	0.104	35.6	6.4e+06	4.5e+10
3.43	-5.02	0.250	37.7	5.3e+06	3.2e+09
5.74	-6.02	0.343	41.1	2.9e+06	1.2e+09
13.1	-7.02	0.612	45.1	7.9e+06	2.2e+08
7.38	4.98	0.367	81.4	5.7e+06	1.0e+09
-6.90	0.48	0.285	88.8	4.2e+06	2.2e+09
5.74	3.99	0.288	103.3	4.2e+06	2.1e+09
5.74	0.48	0.237	105.1	4.3e+06	3.7e+09
-3.38	-1.52	0.153	140.4	1.3e+07	1.4e+10
-4.04	-3.52	0.221	173.8	1.1e+07	4.6e+09

[a] Angular offset from Sgr A* of the center of the detected clump. [b] Projected angular distance from Sgr A*. [c] Minimun number density required to sustain against the tidal shear; $n_{min} = 5 \times 10^7 d^{-3}$.

molecular cloud located at a relatively large distance from Sgr A*. The massive star formation could be triggered by cloud-cloud collision because it can easily make high-mass stars (e.g. Tsuboi et al. 2015). In addition, the cloud has considerably lost its angular momentum owing to the head-on collision. Consequently, the star-forming cloud has fallen into the immediate vicinity of Sgr A* with the time scale of $\sim 10^5$ yr, comparable to the expected growth time of massive stars by accretion (e.g. Krumholz et al. 2008) Now the falling cloud is being disrupted by the tidal shear of Sgr A* and the molecular gas in the cloud is ionized by UV continuum from the OB stars of the Central cluster. This is identified as the Mini-spiral. Because the period of the circular orbit around Sgr A* is $0.2 - 2 \times 10^4$ yrs at $R = 0.1 - 0.5$ pc (see Table 2), the shearing motion would wind the Mini-spiral around Sgr A* closely within $\sim 10^4$ yrs. Although massive stars evolve quickly, low mass stars should be still on the stage of protostar. They may be the sources with a bow-shock appearance observed by JVLA (Yusef-Zadeh et al. 2015a). A part of the massive stars formed in the cloud may be captured in the

vicinity of Sgr A* and participate in the Central cluster. The captured stars probably form a disk-like structure (Cf. Saitoh et al. 2014). This is consistent with the observed disk-like distributions of the Central cluster (e.g. Paumard et al. 2006).

Acknowledgments

We would like to acknowledge Dr. S. Nishiyama at Miyagi University of Education for useful discussion. The National Radio Astronomy Observatory is a facility of the National Science Foundation operated under cooperative agreement by Associated Universities, Inc. USA. This paper makes use of the following ALMA data: ADS/JAO.ALMA#2011.0.00887.S. ALMA is a partnership of ESO (representing its member states), NSF (USA) and NINS (Japan), together with NRC (Canada), NSC and ASIAA (Taiwan), and KASI (Republic of Korea), in cooperation with the Republic of Chile. The Joint ALMA Observatory is operated by ESO, AUI/NRAO and NAOJ.

References

Brinkerink, C. D., et al. 2015, A&A, 576, 41

Christopher, M. H., Scoville, N. Z., Stolovy, S. R., & Yun, Min S., 2005, ApJ, 622, 346

Ekers, R. D., van Gorkom, J. H., Schwarz, U. J., & Goss, W. M., 1983, A&A, 122, 143

Figer, D. F.; McLean, I. S., & Morris, M., 1999, ApJ, 514, 202

Figer, D. F. et al. 2002, ApJ, 581, 258

Genzel, R., Thatte, N., Krabbe, A., Kroker, H., & Tacconi-Garman, L. E. 1996, ApJ, 472, 153

Ghez, A. M., et al. 2008, ApJ, 689, 1044

Gillessen, S., Eisenhauer, F., Trippe, S., Alexander, T., Genzel, R., Martins, F.,& Ott, T. 2009, ApJ, 692, 1075

Hildebrand, R. H., 1983, QJRAS, 24, 267

Krumholz, M. R., Klein, R. I., McKee, C. F., Offner, S. S. R., & Cunningham, A. J., 2007, Science, 5915, 754.

Lo, K.Y. & Claussen, M. J., 1983, Nature, 306, 647

Lu, J. R., Do, T., Ghez, A. M., Morris, M. R., Yelda, S., & Matthews, K. 2013, ApJ, 764, id155

Maness, H. et al. 2007, ApJ, 669, 1024

Morris, M.,& Serabyn, E. 1996, AAR&A, 34, 645

Paumard, T., et al. 2006, ApJ, 643, 1011

Saitoh, T. R. et al. 2014, PASJ, 66, id1

Sanchez-Bermudez, J. Schödel, R., Alberdi, A., Mužič, K., Hummel, C. A., & Pott, J. U. 2014, A&A, 567, A21

Schödel, R., . Eckart, A, Iserlohe, C., Genzel, R. & Ott, T., 2005, ApJ, 625, L111

Tsuboi, M., Tadaki, K-I., Miyazaki, A., & Handa, T. 2011, PASJ, 63, 763

Tsuboi, M., Miyazaki, A., & Uehara, K. 2015, PASJ, 67, id90

Tsuboi, M., Miyazaki, A., & Uehara, K. 2015, PASJ, 67, id109

Williams, J. P., de Geus, E. J. & Blitz, L. 1994, ApJ, 428, 693

Yusef-Zadeh, F., Morris, M. 1987, ApJ, 320, 545

Yusef-Zadeh, F. et al. 2013, ApJ, 767, id L32.

Yusef-Zadeh, F. Roberts, D. A., Wardle, M., Cotton, W., Schödel, R., & Royster, M. J. 2015,ApJ, 801, id. L26

Yusef-Zadeh, F. et al. 2015,ApJ, 808, id. 97

Zhao, J-H, Morris, M. R. Goss, W. M. & Tao, A., 2009, ApJ, 699,186